Three-phase Four-wire Interlinking Converter with Enhanced Power Quality Improvement Feature in Microgrid Systems

Jiannan Liu, *Member, IEEE,* Seyedfoad Taghizadeh, *Member, IEEE,* Junwei Lu, *Senior Member, IEEE,* M. J. Hossain, *Senior Member, IEEE,* Sascha Stegen, *Member, IEEE,* Hui Li, *Member, IEEE*

***Abstr[1]act*— This paper presents an advanced three-phase four-wire interlinking microgrid system with improved harmonics reduction feature. Due to the robustness and simplicity features, the time-domain second-order notch-filter equivalent techniques have drawn a great deal of research attention. However, the drawbacks of non-satisfactory harmonics rejection characteristics and dynamic response limit their applications. In this context, this paper proposes an advanced control system with an enhanced harmonics reduction feature for a microgrid application. The proposed control system exhibits superior harmonics reduction feature and better dynamic response than the conventional notch-filter based techniques. In addition, a control scheme is developed for a three-phase power system application which presents higher accuracy in compensating both balanced and unbalanced harmonics. The performance of the proposed system is validated through simulations and tested on the hardware of a real microgrid system. From the results, it is evident that the proposed scheme provides excellent performance in terms of harmonics reduction in microgrid systems.**

***Index Terms*—grid-connected microgrid, harmonics reduction, notch filter, power management**

NOMENCLATURE

APF	active power filter
SOGI	second-order generalised integrator
SRF	stationary reference frame
STATCOM	static compensator
LC	inductor-capacitor
LCL	inductor-capacitor-inductor
THD	total harmonics distortion
DG	distributed generation
PV	photovoltaic
EAF	enhanced adaptive filter
OSG	orthogonal signal generator
PLL	phase-locked loop
LV	low voltage
PI	proportional integral
AC	alternative current
DC	direct current
P_m	microgrid output active power
Q_m	microgrid output reactive power
P_h	active power loss caused by harmonics
Q_h	reactive power loss caused by harmonics
P_{ref}	reference active power
Q_{ref}	reference reactive power
u_{od}, u_{oq}	rotational voltage control signals
i_{od}, i_{oq}, i_{o0}	rotational current control signals
i_{hd}, i_{hq}, i_{h0}	rotational harmonic current control signals
i_d^*, i_q^*	rotational reference frames of microgrid current
i_{od}^*, i_{oq}^*	rotational reference frames of power current
v_{id}^*, v_{iq}^*, v_{i0}^*	rotational harmonic current control signals
ω	microgrid angular frequency
L_m	filter inductor
K_{pc}	proportional gain of PI controller
K_{ic}	integral gain of PI controller
k	notch filter bandwidth coefficient
i_{fa}, i_{fb}, i_{fc}	three-phase current fundamental components
i_{ha}, i_{hb}, i_{hc}	three-phase harmonics current components
i_{la}, i_{lb}, i_{lc}	three-phase load currents
K_{1a}, K_{1b}, K_{1c}	estimated amplitudes of the sine terms
K_{2a}, K_{2b}, K_{2c}	estimated amplitudes of the cosine terms
μ_1, μ_2	learning rate of the controller
f	microgrid frequency
T	time constant of the low pass filter
γ_{od}, γ_{oq}, γ_{o0}	rotational state variables

I. INTRODUCTION

A. Motivation and Incitement

The microgrid concept is proposed as a solution to integrate distributed energy resources into the utility grid and overcome their intermittency, and variable outputs drawbacks [1]. Among the various aspects of microgrids, improving power quality, especially harmonics, has drawn a great deal of attention [2].

Basically, there are two primary harmonic sources in the power grids, including power electronic devices and non-linear loads [3]. The power electronic devices are widely used for applications such as rectifiers, inverters, static compensators (STATCOMs) and microgrid interlinking converters [4]. In order to reduce the harmonics generated by the power electronic converters, inductor-capacitor (*LC*) or inductor-capacitor-inductor (*LCL*) filters are commonly used to mitigate the high-frequency harmonics orders. However, non-linear loads exhibit different behaviours. They demand harmonics that are supposed to be generated by the utility grid. Although the loads could operate normally in this way, the distorted network current increases the total harmonics distortion (THD) of the grid voltage and current. This leads to extra power loss and may harm some installed equipment. Therefore, it is necessary to keep the THD level within an acceptable range based on the grid standards. According to IEEE standard 1547 or Australian standard 4777, the total current distortion should be less than 5% [5, 6].

With the widespread of microgrid application and the

DOI: 10.17775/CSEEJPES.2020.01850

increasing demand for harmonics suppression, it is possible to combine the two concepts together in order to build a microgrid with harmonics rejection function for the utility network. In this case, the microgrid shall be able to achieve the energy-saving and power quality improvement for the grid simultaneously without introducing other types of equipment or elements.

B. Literature Review

The most commonly used solution to suppress the harmonics of the grid is to utilise active power filter (APF) near to the loads. APF is a shunt-connected power electronic device, which can generate the opposite harmonics to the grid and cancel the distortions of the grid-side current. An APF includes an outer harmonics detection control algorithm, which operates in time-domain or frequency-domain to extract the harmonics and generates reference signals for the inner current control loop.

APF is used in the control system of single-phase converters used for interconnection of distributed generation (DG) units in [7, 8]. In [9], a voltage-control based harmonics rejection method is integrated with a photovoltaic (PV) interfacing inverter, which utilises the inverter as a virtual harmonic resistance to damp the harmonics orders. Authors in [10, 11] introduced the support vector machine method for low-order harmonics mitigation. In [12], a current-control based harmonics detection method is used in the control system of a PV inverter to compensate for the specific order of harmonics as well as to generate active power, which is originated from the PV panel. These control strategies compensate for the specific orders of harmonics (mainly low-order harmonics), which complicates the calculation and the implementation. It is commonly recommended to apply a simple and robust current loop for the removal of the low-order harmonics [13]. The complexity feature of the aforementioned control methods may affect the robustness of the whole system to a great extent.

Various frequency-domain and time-domain harmonics detection methods are reviewed in [14, 15]. Among those techniques for single-phase applications, the second-order notch-filter equivalent methods have shown robustness, low-computation and simplicity for implementation [16]. The stationary reference frame (SRF) harmonics generation and the second-order generalised integrator (SOGI) are the most popular notch-filter equivalent methods, which are well-suited for industrial applications [17]. However, the main drawbacks of these methods are their non-sufficient harmonics rejection characteristic and dynamic response. To overcome these problems, an enhanced adaptive filter (EAF) is proposed in [18] in the design of an orthogonal signal generator (OSG) for a single-phase converter. The EAF method shows higher disturbance rejection capability and quicker response than the notch-filter equivalent methods (i.e. SOGI and SRF) by taking advantage of its third-order transfer function. Nevertheless, all these methods mainly focus on single-phase applications, where unlike the three-phase applications; the voltage and the current are not vulnerably exposed to unbalanced conditions.

Among the three-phase APFs for microgrids, authors in [19] build a hierarchical control system for the grid-connected microgrid to improve the power quality of the network. This work mainly aims to optimise the harmonics caused by the unbalanced voltage scenario, which occurs between the distorted grid and the microgrid due to the droop control characteristic. However, dealing with the harmonics caused by the non-linear loads is not addressed in this research. The non-linear loads' impact on the grid is as serious as the microgrid side. Authors in [20, 21] summarised the load forecasting methods, which present good direction for non-linear loads' prediction. Such methods could be utilised to predict the loads' harmonics while with multiple links. However, in the universal power systems, the demand for real-time control could be fulfilled by the modern measurement devices (e.g. current sensors). Authors in [22] achieve a current waveform optimisation within the microgrid system while they propose an additional APF, operating based on voltage detection techniques. Although the APF compensates for the harmonics, the added APF is an additional device, which increases the complexity, the volume and the cost of the whole microgrid system. Moreover, the presented APF is designed and tested when the harmonics of the three phases are at the same level (balanced harmonics), while in a real application the three phases might have different THDs named unbalanced harmonics in this paper. Authors in [23] combine the PV inverter and the APF together for a three-phase system application. The typical SRF method is utilised in [23] for harmonics detection. Although the controller's configuration is simple, however, it can only be effective to a limited extent due to the inaccuracy of the used low-pass filters. Hamid et al. considered the non-linear loads' effect in the microgrid power system in [24-26]. The researchers intelligently proposed a droop control based control strategy for the microgrid in order to regulate the voltage THD to a low level. The proposed control method also presents excellent performance for the unbalanced loads' condition. In addition, the neural network concept is adopted for harmonics detection. The entire research work has been improved several times and forms a mature controller for the microgrid to solve the power quality issue of the grid side [27]. However, the controller refers to quite a number of theories and dramatically expands the amount of calculation. The method is more suitable for a multi-microgrid system with hierarchical control and grid support requirements. Authors in [28] propose a three-phase APF including three single-phase full-bridge converters, which are controlled separately. The proposed APF approach in [28] uses three individual single-phase control systems to control the current of each phase separately. As a result, this APF is able to compensate for unbalanced harmonics of the three phases, but with the expense of extra work on the controller (three phase-locked-loops, three OSG blocks, three $\alpha\beta/dq$, three $dq/\alpha\beta$ transformation, etc.) and extra hardware (12 switches).

According to the reported research work, it is expected to achieve the harmonics rejection within a microgrid with the following demands:

- A simple structure of the controller with a good robustness feature.
- Applicable to a three-phase power system considering unbalanced harmonics and unbalanced loads cases.
- An independent harmonics rejection function which has no impact on the bi-directional power management operation of the microgrid.

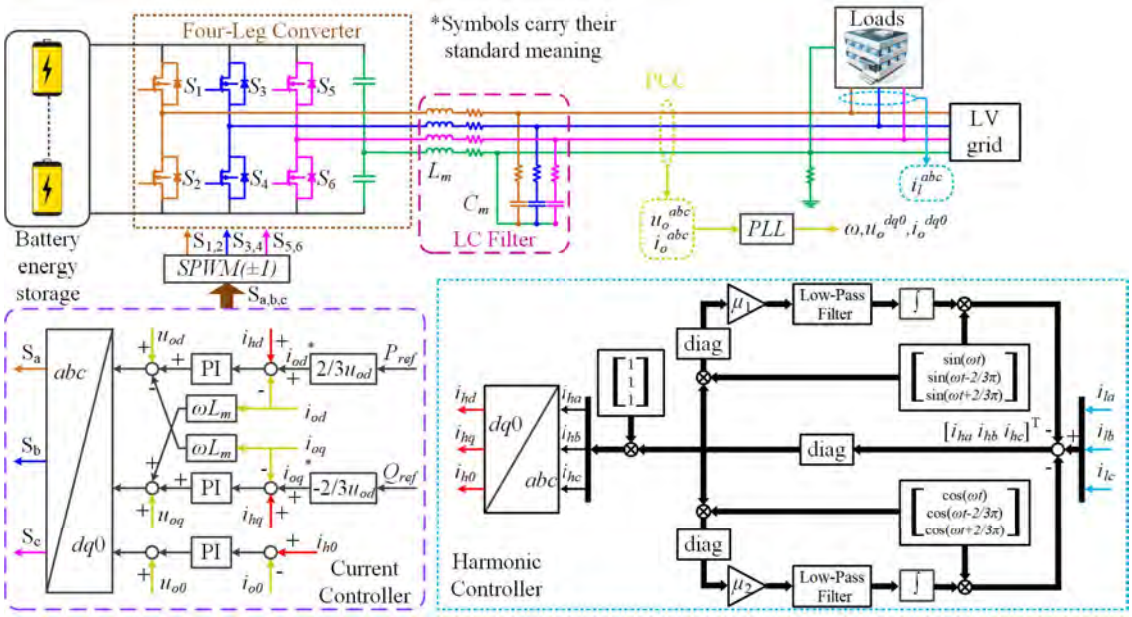

Fig. 1. Three-phase four-wire grid-connected microgrid system with the proposed control strategy.

C. Contribution and Paper Organisation

This paper proposes an advanced three-phase four-wire microgrid interlinking converter with an upgraded power quality feature. The proposed harmonics reduction approach is developed in the context of the method presented in [18] and utilised for the three-phase four-wire interlinking converter application. The method introduced in [18] has been utilised for an ideal single-phase application. Moreover, the areas of the unbalanced conditions, which are very common in a three-phase application, is not taken into account. These motivate this paper to develop and configure this simple and reliable method for a four-leg split-capacitor topology controlled by *dq*0 transformation control algorithm. The proposed approach exhibits higher harmonics rejection capability and better dynamic response than the notch-filter equivalent methods followed by more accuracy in compensating both balanced and unbalanced harmonics. The advantages of the proposed control system are listed as follows:

- Higher disturbance rejection characteristics than the conventional notch-filter equivalent methods.
- Better dynamic response than the conventional notch-filter equivalent methods.
- Higher accuracy in compensating balanced and unbalanced three-phase harmonics.

The rest of the paper is organised as follows. Section II presents the microgrid system with the proposed control strategy. The controller is described and analysed mathematically in detail. Section III proves the controller's stability according to the root locus theory. Simulation and experimental results under different scenarios are provided in Section IV and Section V, respectively, to show the performance of the proposed controller. Section VI makes a discussion based on the gathered results. Section VII summarises the conclusion of the paper and proposes some expectations for the authors' future work.

II. System Configuration and Proposed Control Strategy

The designed system with its control method is shown in Fig. 1. A battery unit is connected to commercial building loads and a low-voltage (LV) network through an interlinking converter, which uses an *LC* filter. The batteries are energy storages for managing bidirectional power flow as well as maintaining a stable direct-current-link (DC-link) voltage. The converter is designed with a four-arm configuration including three transistor-bridge arms and a split-capacitors bridge. The neutral line is drawn from the midpoint of the split capacitors so that the converter is able to supply single-phase loads. In addition, such a configuration physically achieves the three phases decoupling since each arm can be viewed as a single-phase half-bridge converter with the combination of the capacitor arm [29].

A. Power Control

As long as the microgrid is connected to the utility network, it is capable of operating as a slave generator, which follows the grid frequency and voltage level. A direct-quadrature (*dq*) decoupled current controller is used to control the active and reactive powers.

According to the instantaneous power theory, the active output power and reactive power meet the following relationship [30]:

$$\begin{cases} P_m + P_h = 3/2(u_{od}i_{od} + u_{oq}i_{oq} + u_{od}i_{hd} + u_{oq}i_{hq}) \\ Q_m + Q_h = 3/2(u_{oq}i_{od} - u_{od}i_{oq} + u_{oq}i_{hd} - u_{od}i_{hq}) \end{cases} \quad (1)$$

where P_m and Q_m are the expected output active and reactive powers, respectively; P_h and Q_h are the active and reactive power loss caused by harmonics from the load side. Since the reference frame is synchronised with the utility network, u_{oq} becomes zero [31]. As a result, (1) can be rewritten as:

$$\begin{cases} P_m + P_h = 3u_{od}i_{od}/2 + 3u_{od}i_{hd}/2 \\ Q_m + Q_h = -3u_{od}i_{oq}/2 - 3u_{od}i_{hq}/2 \end{cases} \quad (2)$$

Therefore, it is possible to control the power outputs by setting the references P_{ref} for active power and Q_{ref} for reactive power at the expected values. However, the harmonics power loss is

unpredictable and cannot be determined through the setting. As a consequence, the reference current in the rotating coordination can be expressed as follows:

$$\begin{cases} i_d^* = i_{od}^* + i_{hd} = 2P_{ref}/3u_{od} + i_{hd} \\ i_q^* = i_{oq}^* + i_{hq} = -2Q_{ref}/3u_{od} + i_{hq} \end{cases} \quad (3)$$

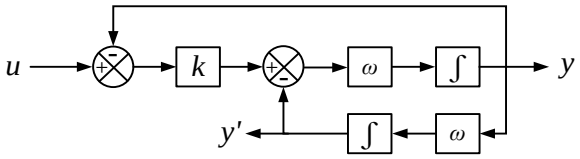

Fig. 2. The control algorithm of SOGI method.

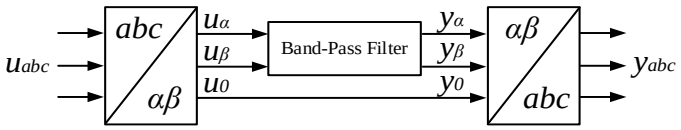

Fig. 3. The control algorithm of SRF method.

B. Conventional Notch-Filter Equivalent Harmonics Reduction Methods

As mentioned before, the notch-filter equivalent algorithms have shown robustness, less computation and simplicity of implementation, which turn them into reliable alternatives for industrial APF applications. In this section, two of the well-known methods, SOGI and SRF are presented.

The control algorithm of SOGI is shown in Fig. 2. The method includes two integrals, which make the system second-order, and a gain k that adjusts the trade-off between the dynamic response and disturbance rejection capability of the SOGI algorithm. The design details and optimum tuning of the SOGI algorithm is presented in Section IV-A.

The control algorithm of the SRF method is illustrated in Fig. 3. This method transforms the three-phase alternative current (AC) waveforms into stationary reference frames ($\alpha\beta$). By using band-pass filters, the harmonics are damped in order to generate the fundamental components ($y_{\alpha\beta}$) of the input waveforms $u_{\alpha\beta}$. Although the mathematical calculation and implementation process of the two methods (i.e. SOGI and SRF) are different, they exhibit the same notch-filter transfer function as given by

$$\frac{u(s)-y(s)}{u(s)} = \frac{s^2+\omega^2}{s^2+k\omega s+\omega^2} \quad (4)$$

where ω is the centre frequency, and k determines the bandwidth of the notch filter. According to the equation, the following rules are abided by 1) If k increases, the speed of (4) increases with the expense of reducing the harmonics reduction feature; 2) On the other hand, reducing k improves the harmonics reduction feature while reducing the rapidity. Based on this law, an optimum design for (4) is to select k = 1.345 according to the analysis in [18] which concludes that the notch filter exhibits lack of optimum harmonics reduction and dynamic response (i.e. overshoot, undershoot and settling time) even at its best tuning (k = 1.345).

C. Proposed Control System Including the Enhanced Harmonics Control Strategy

The configuration of the harmonics detection algorithm is shown in Fig. 1. Taking single-phase current $i(t)$ as an example, since the current waveform is supposed to follow a sine wave trend, its fundamental component $i_f(t)$ can be expressed as [18, 32]:

$$i_f(t) = K_1(t)\sin(\omega t) + K_2(t)\cos(\omega t) \quad (5)$$

where $K_1(t)$ and $K_2(t)$ are the constant estimations for the sine and cosine terms. ω is the angular frequency of the grid voltage. Since the detection is for a three-phase system, the harmonic currents

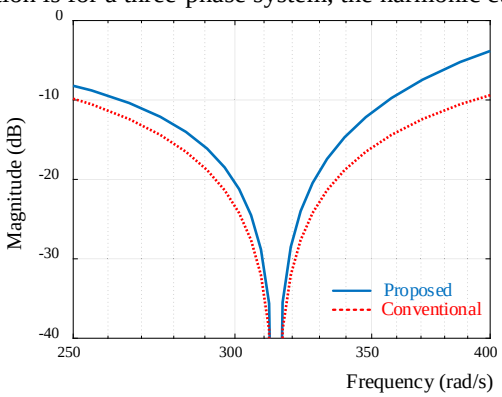

Fig. 4. The frequency response of the proposed method and the SOGI method: a) in generating $u_\alpha(t)$ and $\acute{u}_\alpha(t)$, b) in generating $u_\beta(t)$ and $\acute{u}_\beta(t)$.

are converted into a diagonal matrix (diag) for calculation purposes. The fundamental components i_f^{abc}(t) of the load currents i_l^{abc}(t) can be expressed as:

$$\begin{bmatrix} i_{fa}(t) \\ i_{fb}(t) \\ i_{fc}(t) \end{bmatrix} = \begin{bmatrix} K_{1a}(t)\sin(\omega t) \\ K_{1b}(t)\sin\left(\omega t - \frac{2}{3}\pi\right) \\ K_{1c}(t)\sin\left(\omega t + \frac{2}{3}\pi\right) \end{bmatrix} + \begin{bmatrix} K_{2a}(t)\cos(\omega t) \\ K_{2b}(t)\cos\left(\omega t - \frac{2}{3}\pi\right) \\ K_{2c}(t)\cos\left(\omega t + \frac{2}{3}\pi\right) \end{bmatrix} \quad (6)$$

where $K_1^{abc}(t)$ and $K_2^{abc}(t)$ are the estimated amplitudes of the sine and cosine terms. The Gradient Descent method is utilised to determine $K_1^{abc}(t)$ and $K_2^{abc}(t)$ [32]. Therefore, $K_1^{abc}(t)$ and $K_2^{abc}(t)$ are obtained from the following equations:

$$\begin{bmatrix} \dot{K_{1a}}(t) \\ \dot{K_{1b}}(t) \\ \dot{K_{1c}}(t) \end{bmatrix} = \mu_1 \begin{bmatrix} i_{ha}(t) & 0 & 0 \\ 0 & i_{hb}(t) & 0 \\ 0 & 0 & i_{hc}(t) \end{bmatrix} \begin{bmatrix} \sin(\omega t) \\ \sin\left(\omega t - \frac{2}{3}\pi\right) \\ \sin\left(\omega t + \frac{2}{3}\pi\right) \end{bmatrix} \quad (7a)$$

$$\begin{bmatrix} \dot{K_{2a}}(t) \\ \dot{K_{2b}}(t) \\ \dot{K_{2c}}(t) \end{bmatrix} = \mu_2 \begin{bmatrix} i_{ha}(t) & 0 & 0 \\ 0 & i_{hb}(t) & 0 \\ 0 & 0 & i_{hc}(t) \end{bmatrix} \begin{bmatrix} \cos(\omega t) \\ \cos\left(\omega t - \frac{2}{3}\pi\right) \\ \cos\left(\omega t + \frac{2}{3}\pi\right) \end{bmatrix} \quad (7b)$$

where $i_h^{abc}(t)$ is the difference between $i_l^{abc}(t)$ and $i_f^{abc}(t)$ and represents for all-order harmonics of phases; and μ=μ_1=μ_2 is the learning rate of the algorithm. By applying the algorithm to the three phases, the three-phase harmonics i_h^{abc} can be detected.

This method, which has a simple structure, is a third-order system with a transfer function, representing for one phase, as given by

$$\frac{i_{ha}(s)}{i_{la}(s)} = \frac{(s^2+\omega^2)}{s^2+\frac{1}{(1+Ts)}\mu s+\omega^2} \quad (8)$$

where μ estimates the bandwidth of the proposed method and T is the time constant of the low pass filter. The proposed method can be designed with either a fixed or an adaptive frequency by receiving the measured frequency from the existing phase-locked loop (PLL). Similar to the notch-filter equivalent SOGI method, the proposed method is simple in structure; thus, it is easy to implement on non-advanced microcontrollers. However, compared with the notch-filter based methods, the proposed method exhibits a better dynamic response (less settling time) as well as a higher disturbance rejection capability, which is

validated through the bode-plots in Fig. 4.

As Fig. 4 shows, using the optimum design for the transfer functions of the proposed method (μ = 314.1, T = 1.44*10^{-3}) and the notch-filter transfer function (k = 1.345) according to [18], the proposed system exhibits a narrower area near the centre frequency f = 314.15 rad/s, which validates the higher harmonics reduction capability particularly at 3rd, 5th and 7th order harmonics.

Since the current controller is conducted under the rotating reference frame system, it is compulsory to convert the three-phase harmonics into $dq0$ components in order to participate in the current control process. The common derived differential-algebraic equations for the current controller are given as follows [33]:

$$\begin{cases} \dot{\gamma_{od}} = i_{od}^* - i_{od} \\ \dot{\gamma_{oq}} = i_{oq}^* - i_{oq} \\ \dot{\gamma_{o0}} = 0 - i_{o0} \end{cases} \tag{9}$$

$$\begin{cases} v_{id}^* = v_{od} + K_{pc}\dot{\gamma_{od}} + K_{ic}\gamma_{od} - \omega L_m i_{oq} \\ v_{iq}^* = v_{oq} + K_{pc}\dot{\gamma_{oq}} + K_{ic}\gamma_{oq} + \omega L_m i_{od} \\ v_{i0}^* = v_{o0} + +K_{pc}\dot{\gamma_{o0}} + K_{ic}\gamma_{o0} \end{cases} \tag{10}$$

where $\dot{\gamma_{od}}$ and $\dot{\gamma_{oq}}$ are the state variables corresponding to the current control proportional-integral (PI) controller; K_{pc} and K_{ic} are the proportional and the integral gains respectively; and v_{id}^*, v_{iq}^* and v_{i0}^* are the reference signals for the sinusoidal pulse width modulation (SPWM) generator. By using the current controller, the $dq0$ output current components i_{od}, i_{oq} and i_{o0} will follow the reference values to control the output powers. According to (9), the reference current is from the power control while the harmonics compensation is not taken into consideration. By modifying the reference current from the power control only to the power control with harmonics compensation, the converter's output current shall possess the ability to compensate the harmonics as well as to generate power to the grid. Thus, through considering the harmonics components i_{hd}, i_{hq} and i_{h0}, (9) can be revised as:

$$\begin{cases} \dot{\gamma_{od}} = i_d^* - i_{od} = i_{od}^* + i_{hd} - i_{od} \\ \dot{\gamma_{oq}} = i_q^* - i_{oq} = i_{oq}^* + i_{hq} - i_{oq} \\ \dot{\gamma_{o0}} = i_{h0} - i_{o0} \end{cases} \tag{11}$$

The reference output signals in the $dq0$ frames need to be reversely converted into the three-phase stationary coordinate system for the SPWM. As a result, each arm of the interlinking converter can be controlled separately to satisfy the power demand and harmonics compensation in each phase.

The proposed harmonics detection algorithm incorporated with the $dq0$ control strategy and the split-capacitor topology is able to achieve a high-accuracy compensation for balanced and unbalanced harmonics with different levels. The converter is designed as a four-leg converter. The three transistor-arm bridges are connected to the three-phase ac power system for power exchange. The fourth leg uses split-capacitor leg instead of transistor leg for the neutral power point utilisation. Since the split-capacitor leg provides the path for the energy to flow for all the three phases, each leg of the converter becomes an independent single-phase half-bridge converter [28]. Therefore, each leg is able to generate independent current output without causing any effect on the other phases. For the unbalanced case, including unbalanced loads and/or unbalanced harmonics, the proposed system shall be able to fulfil the supply requirement.

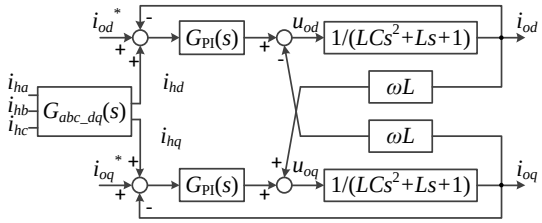

Fig. 5. Block diagram of the controller and plant in dq frame.

III. Controller Stability Analysis

In this section, the stability of the proposed control strategy is analysed based on root locus theory. As described in Section II, the transfer function of the proposed enhanced harmonics controller $G_{\mathrm{EHC}}(s)$ is given by

$$G_{\mathrm{EHC}}(s) = \begin{bmatrix} \frac{(s^2+\omega^2)}{s^2+\frac{1}{(1+Ts)}\mu_a s+\omega^2} & 0 & 0 \\ 0 & \frac{(s^2+\omega^2)}{s^2+\frac{1}{(1+Ts)}\mu_b s+\omega^2} & 0 \\ 0 & 0 & \frac{(s^2+\omega^2)}{s^2+\frac{1}{(1+Ts)}\mu_c s+\omega^2} \end{bmatrix} \tag{12}$$

Since the harmonics references should be transformed from the three-dimensional stationary coordinate system to the two-dimensional rotating system through Clarke transformation, the transfer functions of the transformation can be represented by

$$G_{abc\_dq}(s) = \frac{2}{3}\begin{bmatrix} \frac{s}{s^2+\omega^2} & -\frac{s-\sqrt{3}\omega}{2(s^2+\omega^2)} & -\frac{s+\sqrt{3}\omega}{2(s^2+\omega^2)} \\ -\frac{\omega}{s^2+\omega^2} & \frac{\sqrt{3}s+\omega}{2(s^2+\omega^2)} & \frac{\sqrt{3}s-\omega}{2(s^2+\omega^2)} \end{bmatrix} \tag{13}$$

The system in this paper employs LC filter. Therefore, the LC filter's transfer function is given by $1/G_{LC}(s) = 1/(LCs^2 + Ls + 1)$. Accordingly, the controllers and plant are shown in Fig. 5. $G_{\mathrm{PI}}(s)$ is the transfer function of the PI controller given by $G_{\mathrm{PI}}(s) = K_p + K_i/s$. From Fig. 5, the transfer function between the input currents and the output currents can be represented as:

$$\begin{bmatrix} i_{od}(s) \\ i_{oq}(s) \end{bmatrix} = \frac{G_{\mathrm{PI}}(s)}{\{[G_{LC}(s)+G_{\mathrm{PI}}(s)]^2+(\omega L)^2\}} \times \begin{bmatrix} G_{LC}(s)+G_{\mathrm{PI}}(s) & -\omega L \\ \omega L & G_{LC}(s)+G_{\mathrm{PI}}(s) \end{bmatrix} \times \begin{bmatrix} i_{dr}(s) \\ i_{qr}(s) \end{bmatrix} \tag{14}$$

where $\begin{bmatrix} i_{dr}(s) \\ i_{qr}(s) \end{bmatrix} = \begin{bmatrix} i_{od}^*(s) + i_{hd}(s) \\ i_{oq}^*(s) + i_{hq}(s) \end{bmatrix}$. For the convenience of the analysis, $G_1(s)$ and $G_2(s)$ are given by

$$\begin{cases} G_1(s) = \frac{G_{\mathrm{PI}}(s)[G_{LC}(s)+G_{\mathrm{PI}}(s)]}{[G_{LC}(s)+G_{\mathrm{PI}}(s)]^2+(\omega L)^2} \\ G_2(s) = \frac{\omega L G_{\mathrm{PI}}(s)}{[G_{LC}(s)+G_{\mathrm{PI}}(s)]^2+(\omega L)^2} \end{cases} \tag{15}$$

By substituting $G_{\mathrm{PI}}(s)$ and (15) into (14), a simplified expression is calculated as

$$\begin{bmatrix} i_{od}(s) \\ i_{oq}(s) \end{bmatrix} = \begin{bmatrix} G_1(s) & -G_2(s) \\ G_2(s) & G_1(s) \end{bmatrix} \begin{bmatrix} i_{od}^*(s) \\ i_{oq}^*(s) \end{bmatrix} + \begin{bmatrix} G_1(s) & -G_2(s) \\ G_2(s) & G_1(s) \end{bmatrix} G_{abc\_dq}(s) G_{\mathrm{EHC}}(s) \begin{bmatrix} i_{la} \\ i_{lb} \\ i_{lc} \end{bmatrix} \tag{16}$$

Five inputs are participating in the calculation of each current component output. The former part stands for the current controller and plant, which has been widely proved to be stable.

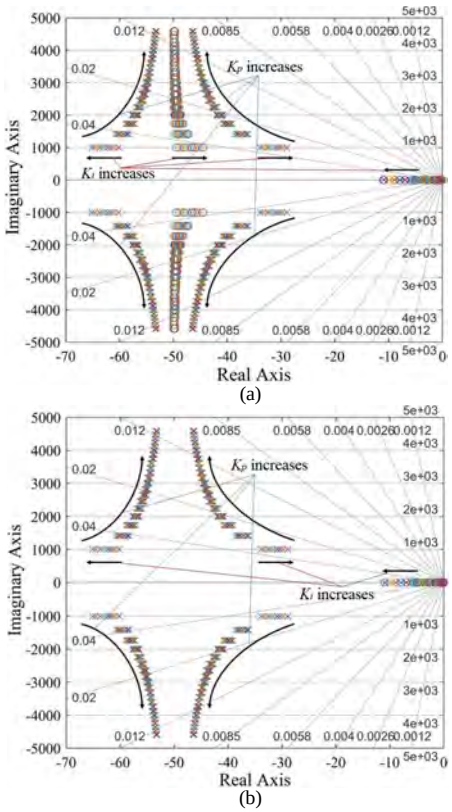

Fig. 6. Root lotus for the i_{la} transfer functions a) corresponding to i_{od}, b) corresponding to i_{oq}.

The latter part represents the proposed harmonics controller combining with the inner current controller and plant. Since $G_{abc\_dq}(s)$ and $G_{EHC}(s)$ are constant in the system, once $G_1(s)$ and $G_2(s)$ are determined to be steady, the latter part should be stable. By taking i_{la}, i_{lb} and i_{lc} as zero respectively, we can get the transfer functions corresponding to each output. In this case, the root locus for the i_{la} transfer functions corresponding to i_{od} and i_{oq} are shown in Fig. 6(a) and Fig. 6(b), respectively. As shown in Fig. 6, all the poles are on the left side of the vertical axis as the K_p and K_i increase from 1 to 1000. The transfer functions of i_{lb} and i_{lc} can also be validated to be stable in this way, which are not covered due to the content repetition. As a result, the transfer functions are stable for all the positive K_p and K_i values according to the poles changing trends appeared in the figures. Thus, according to the superposition theorem, the system is stable for all the positive K_p and K_i values.

IV. Simulation Results and Discussions

In this section, the performance of the designed microgrid interlinking system with its advanced power quality improvement feature is evaluated through the simulations conducted in MATLAB/Simulink under different cases. The simulation model is based on a microgrid system with the parameters summarised in Table I.

A. Performance Evaluation of the Proposed Harmonics Reduction

The aim of this case study is to verify the superior performance of the proposed system. At the same time, it is compared with the conventional notch-filter equivalent techniques (i.e. SOGI and SRF). The proposed and conventional methods are designed with

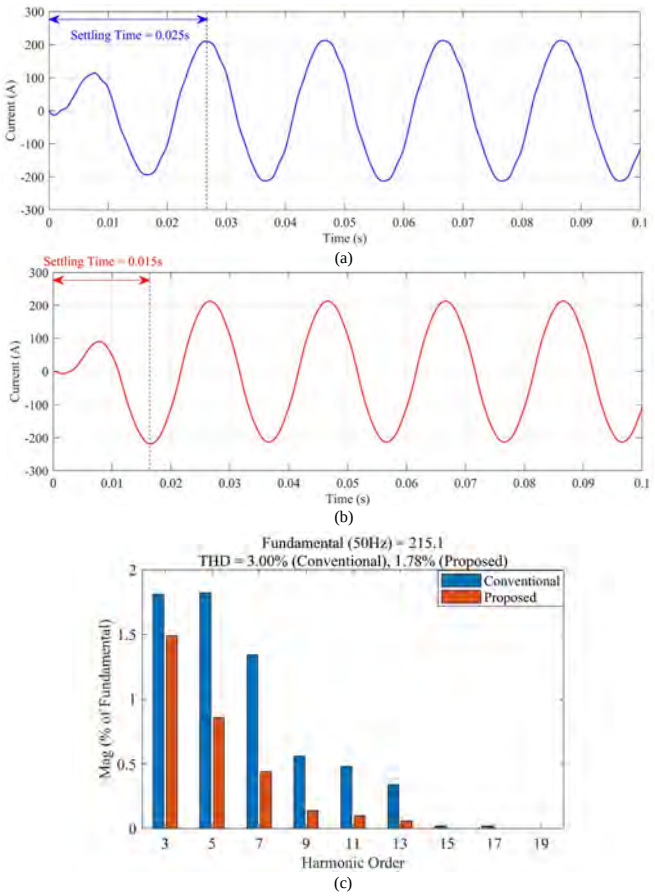

Fig. 7. a) Fundamental component generated by the conventional notch-filter based methods, b) Fundamental component generated by the proposed harmonics reduction method, c) FFT analysis comparison between by the conventional NF and proposed NF.

TABLE I. Simulation Parameters of the Proposed System

System Parameter	Value	Control Parameter	Value
Nominal DC Voltage	800V	K_p	2.5
AC Ph-Ph Voltage	420V	K_i	5
Loads	95kW/54kVar		
L	1mH	Switching Frequency	10kHz
C	1 mF		
Frequency	50Hz		

the gains $\mu = 314.1$, $T = 1.44*10^{-3}$ for the proposed algorithm and $k = 1$ for the conventional notch-filter based techniques. In order to validate the better dynamic response and harmonics reduction capability of the proposed method, the conventional method is designed with a gain value of k slightly less than its optimum design (k = 1.345). This design compared with the optimum design is supposed to exhibit better harmonics reduction capability for the conventional method. Following that the conventional system is supposed to achieve better harmonics reduction capability than its rapidity. However, as the results in Fig. 7 show, the THD of the fundamental component in Fig. 7 (a) generated by the conventional method is higher than the THD of the fundamental component in Fig. 7 (b) using the proposed method.

Moreover, according to the results, the settling time using the proposed system is 0.015 s, while it is 0.025 s when the conventional notch-filter based algorithms are utilised. As aforementioned in Section II-C, although the settling time of the notch-filter method can be reduced via increasing the gain k, this

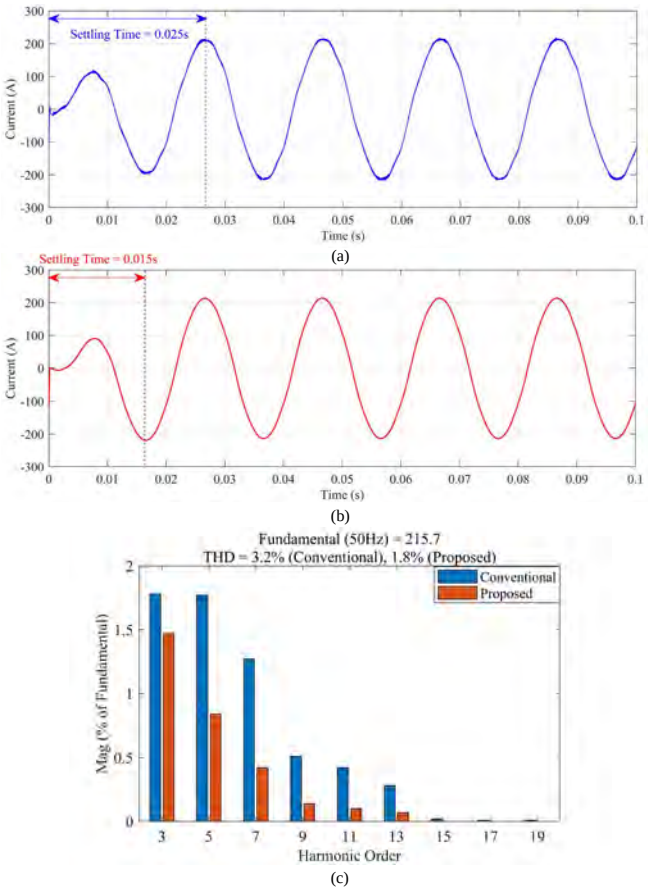

Fig. 8. a) Grid-side current while the conventional notch-filter based methods are used, b) Grid-side current while the proposed method is used, c) FFT analysis comparison between by the conventional NF and proposed NF.

is not desired, since it will worsen the harmonics reduction capability of the algorithm. As a consequence, the harmonics rejection feature of the proposed method is significantly better than the harmonics reduction characteristic of the conventional method at any design, including its optimum design. The results of this test, which validate the bode-plot analysis in Fig. 4, verify both better dynamic response and the harmonics reduction feature of the proposed method. Fig. 7 (c) compares the THD of the generated fundamental component, 1.78%, which exhibits around 40% times lower than the response of the notch filter-based conventional methods.

Fig. 8 (a) shows the quality of the grid-side current when the notch-filter based methods are used in the control system of the microgrid interlinking converter. As can be seen in Fig. 8 (c), the THD of the grid-side current is 3.2%. However, using the proposed system, the THD is reduced to 1.8%. The improved dynamic response of the proposed system can also be validated from the results in Fig. 8 (b). The settling time is around 0.015 s which is less than the 0.025 s in Fig. 8 (a).

For the sake of comparison in the rest of the analysis of this paper, the conventional notch-filter based methods are designed to achieve their optimum performance (k = 1.345).

B. Harmonics Reduction when the Harmonics are Balanced and the Loads are Unbalanced

The objective of this case study is to validate the harmonics reduction performance of the proposed system when the three-phase loads are unbalanced, but the harmonics of the phases are

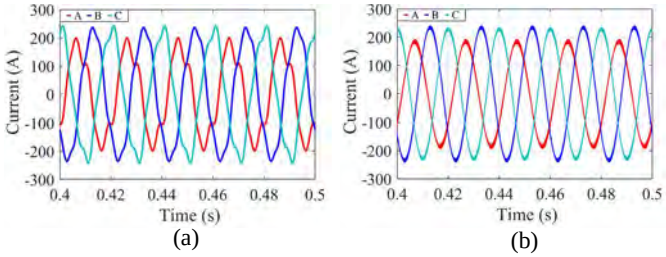

Fig. 9 Three-phase grid currents a) without compensation b) with compensation.

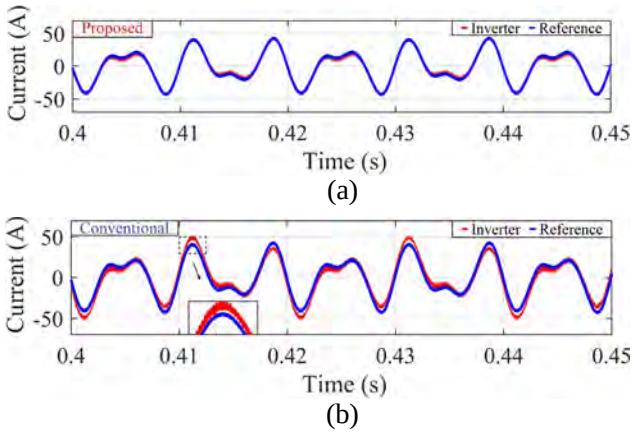

Fig. 10. Harmonics tracking performance (a) proposed three-arm inverter with split-capacitor arm (b) conventional three-arm inverter.

balanced. In Fig. 9 (a), the microgrid interlinking converter is in stand-by mode. In Fig. 9 (b), the proposed harmonics controller is activated, and the current harmonics are minimised without affecting the amplitudes of the phases.

Fig. 10 shows the accuracy of the proposed system compared with the conventional systems. In Fig. 10 (a), using the proposed control system, the output current of the converter can precisely track the harmonic reference signal, whereas using the conventional system in Fig. 10 (b), the outputs of the three phases influence each other making the converter's output exhibit low accuracy to follow the reference. The main reason that the system could achieve better harmonics tracking performance is that the converter is designed as a four-leg converter for the three single-phase loads supply. The three transistor-arm-based bridges are connected to the three-phase ac power system for power exchange. The fourth leg uses a split-capacitor leg instead of transistor leg for the neutral inductor utilisation. Since the split-capacitor leg provides the path for the energy flow for all the three phases, each leg of the converter becomes an independent single-phase half-bridge converter. Therefore, each leg is able to generate independent current output without interfering the other phases. This result validates the higher accuracy of the proposed system in compensating for balanced and unbalanced harmonics levels.

C. Harmonics Reduction when the Harmonics are Balanced and Unbalanced

This test aims to validate the harmonics reduction performance of the proposed system when the three-phase loads are balanced, but the harmonics are conducted balanced and unbalanced separately. In Fig. 11 (a), the three-phase grid currents are distorted with the balanced harmonics, which are shown on the

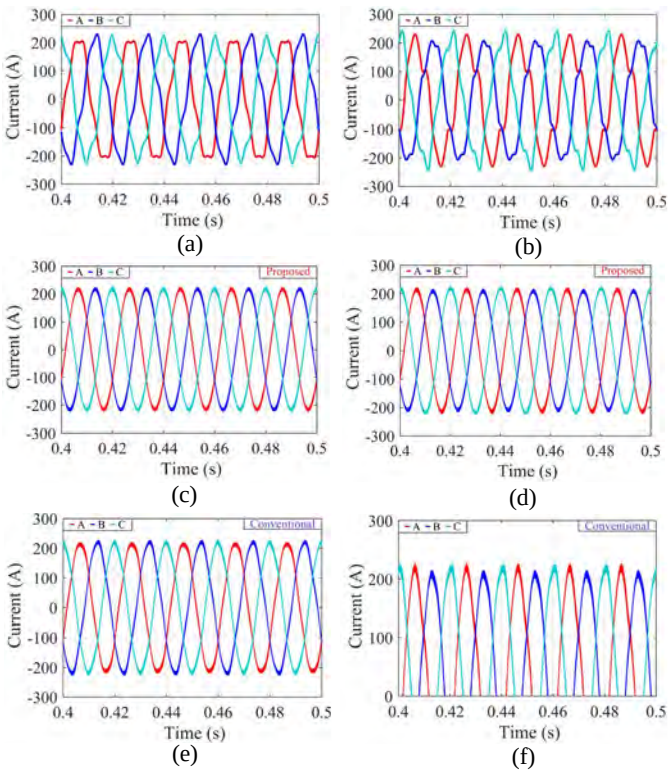

Fig. 11. Three-phase grid currents (a) balanced harmonics without compensation (b) unbalanced harmonics without compensation (c) balanced harmonics with proposed compensation (d) unbalanced harmonics with proposed compensation (e) balanced harmonics with conventional compensation (f) unbalanced harmonics with conventional compensation.

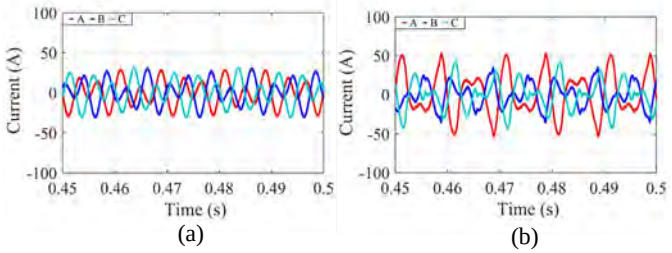

Fig. 12. Grid side harmonic currents (a) balanced harmonics (b) unbalanced harmonics.

TABLE II. TOTAL HARMONICS DISTORTION OF EACH PHASE

Case	Phase	THD without compensation	THD with proposed compensation	THD with conventional compensation
Balanced Harmonics	A	16.25%	1.80%	4.09%
	B	16.33%	1.85%	3.28%
	C	16.38%	1.88%	4.31%
Unbalanced Harmonics	A	20.07%	2.53%	5.20%
	B	11.15%	1.34%	2.79%
	C	18.58%	2.30%	4.98%

grid-side currents in Fig. 12 (a). In Fig. 11 (b), the three-phase grid currents waveforms are distorted with the unbalanced harmonics, which can be seen in Fig. 12 (b). The proposed system precisely compensates both balanced and unbalanced cases, as shown in Fig. 11 (c) and 11 (d), respectively. However, the conventional approach shows mal-operation in balancing the loads, as shown in Fig. 11 (e) and particularly in Fig. 11 (f). In Table II, the THDs of the three-phase currents are listed before and after harmonics compensation. The results indicate the higher accuracy of harmonics reduction performance using the proposed system.

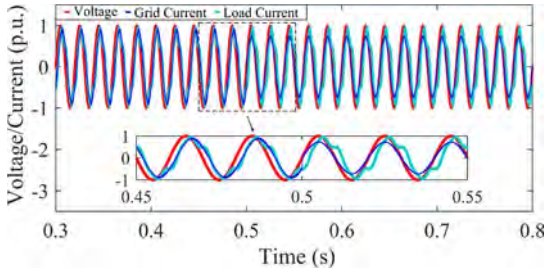

Fig. 13. Reactive power compensation.

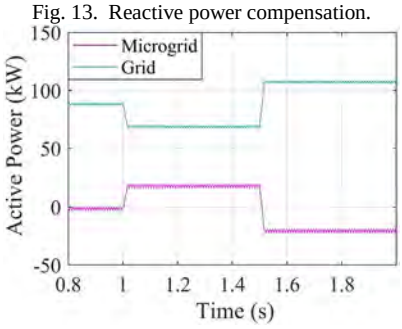

Fig. 14. Active power generation.

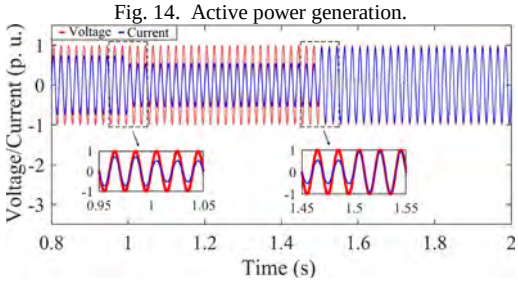

Fig. 15. Single-phase grid current variation due to the active power generation change of the microgrid.

D. Harmonics Reduction with Power Management

In this case study, the operation of the microgrid to supply the simultaneous functions of harmonics reduction and power flow management is tested and verified. Fig. 13 shows the performance when the microgrid starts to compensate reactive power to the grid. The phase angle difference between the grid voltage and the grid current in Phase A is eliminated due to the reactive power compensation. In the context, the grid current amplitude also decreases since the reactive current is completely supported by the microgrid. In the meantime, the microgrid is still compensating the harmonics demanded by the loads.

Fig. 14 shows the active power generation performance from 0.8 s to 2 s. As long as the microgrid starts to output active power, the grid generation decreases so that the energy-saving function is achieved in this way. At 1.5 s there is a requirement for charging the battery; thus, the microgrid will draw active power from the grid. Therefore, the direction of the power changes from positive to negative. Fig. 15 shows the grid voltage and current waveforms during the same time span as Fig. 14. The current is synchronised with the voltage as a sine waveform which means that while the microgrid manages the active power flow, it is able to compensate the reactive power and harmonics simultaneously. The simulation results perfectly demonstrate the simultaneous integration of the bidirectional power management, reactive power compensation and the harmonics reduction functions.

V. EXPERIMENTAL RESULTS AND DISCUSSION

A lab-scale grid-connected microgrid system with the battery

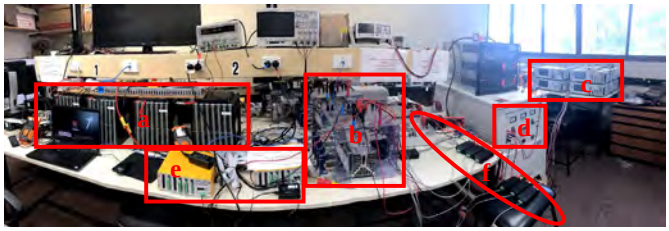

Fig. 16. Grid-connected microgrid system hardware configuration (a) batteries (b) Smart converter (c) Single-phase programmable loads (d) Transformer (e) DSP controller (f) Sensors and filter.

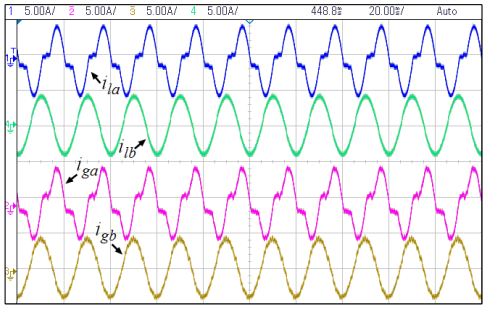

(a)

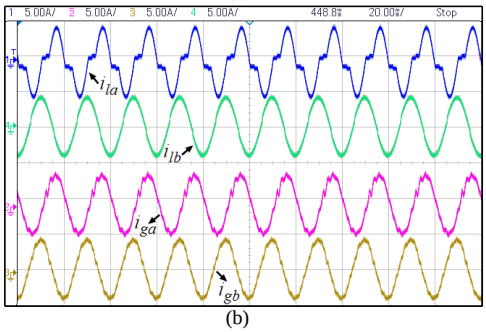

(b)

Fig. 17. Single-phase grid current (a) before compensation (b) after compensation.

and smart inverter is developed, as shown in Fig. 16. Four Kokam batteries, which can offer a total output of 200 V DC voltage, are used. Three Ametek programmable single-phase loads are utilised to provide different load cases and harmonics levels for the testing. A modified four-leg SEMIKRON-IGBT inverter is utilised as the interlinking converter. The control strategy is implemented on a TMS320F28377 DSP based controller through C-language programming. A step-down transformer is utilised to decrease the ac RMS voltage from 420 V to 85 V for experimental testing. The tests are conducted under different cases of balanced and unbalanced harmonics and loads.

A. Single-Phase Harmonics Reduction with Balanced Loads

In this test, Phase A is distorted while the other phases (Phase B and Phase C) do not include harmonics. As shown in Fig. 17 (a), the load current i_{la} in Phase A contains a THD of 31.3%. The three-phase loads demand 3×147 W. With the proposed harmonics compensation, as shown in Fig. 17 (b), the THD of the grid current i_{ga} on Phase A is reduced to 4.45%. This is basically an unbalanced harmonics case in which Phase B and C are not distorted. The grid and the load current of Phase B are also shown for comparison.

B. Double-Phase Unbalanced Harmonics Reduction with Balanced Loads

As shown in Fig. 18(a), both load currents of Phase A and B include different THDs of 21.4% and 36.2% respectively. The grid currents also follow the same THD to meet the load demands.

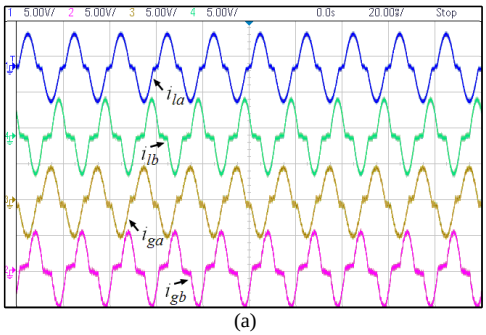

(a)

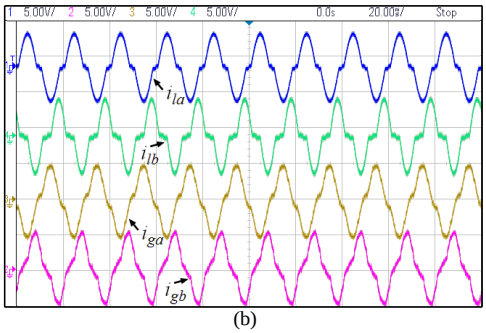

(b)

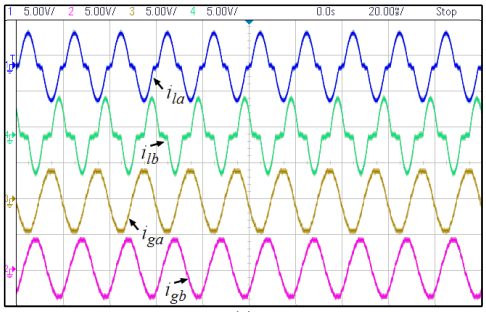

(c)

Fig. 18. Double-phase grid current with different degree of distortion (a) before compensation (b) compensation with conventional method (c) compensation with the proposed method.

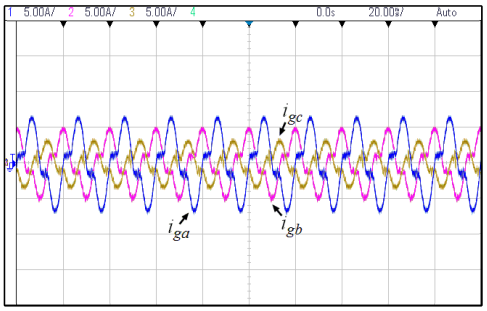

(a)

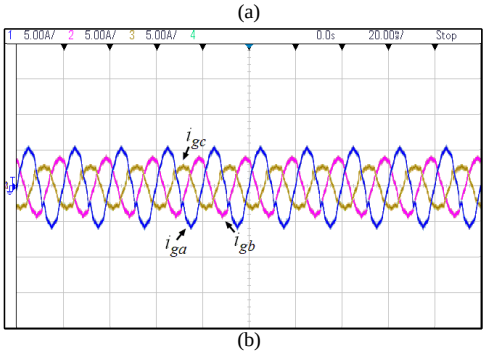

(b)

Fig. 19. Three-phase grid current under unbalanced loads condition (a) before compensation (b) after compensation.

As can be seen in Fig. 18(b), using the conventional method, the harmonics cannot be removed properly. However, with the proposed harmonics compensation in Fig. 18(c), the THD of both phases are reduced to 4.1% and 4.5%, which indicates the compensation for each phase separately without causing any effect on the other phases.

C. Three-Phase Balanced Harmonics Reduction with Unbalanced Loads

This test aims to show the compensation performance under the balanced harmonics and unbalanced loads condition. In this experiment, the loads in Phase A, Phase B and Phase C are 98 W, 147 W and 196 W respectively. The loads are unbalanced while having the same THD of 31.5% as shown in Fig. 19(a). The proposed system is capable of compensating the harmonics in this case, as shown in Fig. 19 (b). The THDs of grid currents after the compensation are 3.9%, 4.1%, 4.9%. Compared to the other two phases, the grid current in Phase C is much smaller due to the load demand. In this case, any noise from the equipment or the grid, even with a small amplitude, could occupy a considerable percentage of the grid current. Therefore, the THD is slightly higher in Phase C, which is because of the inevitable high distortion of a low-current waveform. From the results, it is concluded that the proposed system is robust against changing the load and the harmonics in different phases.

VI. Discussions

The objective of the presented work is to propose an enhanced harmonics rejection feature-based control method for a grid-connected microgrid system to achieve the power quality improvement of the grid as well as to exchange the power with the utility network. The correctness of the research is validated through simulations in MATLAB/Simulink environment and through experiment based on a real microgrid testing benchtop under unbalanced loads and unbalanced harmonics cases. Although the experimental investigation is conducted in a lab-scale level, the proposed method could be further applied to higher-level power systems.

VII. Conclusion

This paper proposes an enhanced control system for a grid-connected three-phase four-wire microgrid interlinking converter. The proposed system exhibits superior performance than the well-known notch-filter equivalent methods in terms of i) improved harmonics rejection characteristic by around 40%, ii) better dynamic response by approximately 50%, and iii) higher accuracy in compensating balanced and unbalanced harmonics level. The proposed harmonics detection method is incorporated with a split-capacitor based four-leg inverter controlled by a *dq*0 current control strategy. The system is simple to implement and stable in operation. The effectiveness and better performance of the proposed system are validated through simulation and experimental results. Although the proposed control strategy is proved to be effective, the distortion factor from the source side is not considered. Therefore, the proposed controller application is limited, considering the source performance, which leads to a future direction of this research. In addition, the controller is tested at a laboratory level. The next step of this research is to apply the proposed method on an industrial microgrid with more and different sources, loads and disturbances.

References

[1] I. U. Nutkani, L. Meegahapola, A. L. P. Chiang and F. Blaabjerg, "Autonomous power management for interlinked AC-DC microgrids," in *CSEE Journal of Power and Energy Systems*, vol. 4, no. 1, pp. 11-18, Mar. 2018.

[2] M. M. Hashempour, T. Lee, M. Savaghebi and J. M. Guerrero, "Real-Time Supervisory Control for Power Quality Improvement of Multi-Area Microgrids," in *IEEE Systems Journal*, vol. 13, no. 1, pp. 864-874, Mar. 2019.

[3] X. Liang and C. Andalib -Bin- Karim, "Harmonics and Mitigation Techniques Through Advanced Control in Grid-Connected Renewable Energy Sources: A Review," in *IEEE Transactions on Industry Applications*, vol. 54, no. 4, pp. 3100-3111, July-Aug. 2018.

[4] A. Tang, Y. Shao, Q. Xu, X. Zheng, H. Zhao and D. Xu, "Multi-objective coordination control of distributed power flow controller," in *CSEE Journal of Power and Energy Systems*, vol. 5, no. 3, pp. 348-354, Sep. 2019.

[5] IEEE Draft Standard Conformance Test Procedures for Equipment Interconnecting Distributed Energy Resources with Electric Power Systems and Associated Interfaces," in *IEEE P1547.1/D9.5, April 2019* , vol., no., pp.1-269, 15 May 2019.

[6] Australian/New Zealand Standard 4777: Grid connection of energy systems via inverters.

[7] X. Sun, J. Zeng and Z. Chen, "Site Selection Strategy of Single-Frequency Tuned R-APF for Background Harmonic Voltage Damping in Power Systems," in *IEEE Transactions on Power Electronics*, vol. 28, no. 1, pp. 135-143, Jan. 2013.

[8] Y. W. Li and J. He, "Distribution System Harmonic Compensation Methods: An Overview of DG-Interfacing Inverters," in *IEEE Industrial Electronics Magazine*, vol. 8, no. 4, pp. 18-31, Dec. 2014.

[9] S. Munir and Y. W. Li, "Residential Distribution System Harmonic Compensation Using PV Interfacing Inverter," in *IEEE Transactions on Smart Grid*, vol. 4, no. 2, pp. 816-827, Jun. 2013.

[10] D. Varajão, R. E. Araújo, L. M. Miranda and J. A. P. Lopes, "Modulation Strategy for a Single-Stage Bidirectional and Isolated AC–DC Matrix Converter for Energy Storage Systems," in *IEEE Transactions on Industrial Electronics*, vol. 65, no. 4, pp. 3458-3468, Apr. 2018.

[11] F. Fang, H. Tian and Y. Li, "SVM Strategy for Mitigating Low Order Harmonics in Isolated AC-DC Matrix Converter," in *IEEE Transactions on Power Electronics*, 2020.

[12] J. He, Y. W. Li, X. Wang and F. Blaabjerg, "An improved current control scheme for grid-connected DG unit based distribution system harmonic compensation," *2013 Twenty-Eighth Annual IEEE Applied Power Electronics Conference and Exposition (APEC)*, Long Beach, CA, pp. 986-991, 2013.

[13] S. Suriana, M. Armstrong, and B. Zahawi. "Randomised integral gain of PI current controller for a single PV inverter system." Engineering, vol. 5, no.1, pp. 221-225, 2013.

[14] L. Asiminoael, F. Blaabjerg and S. Hansen, "Detection is key - Harmonic detection methods for active power filter applications," in *IEEE Industry Applications Magazine*, vol. 13, no. 4, pp. 22-33, July-Aug. 2007.

[15] Y. W. Li and J. He, "Distribution System Harmonic Compensation Methods: An Overview of DG-Interfacing Inverters," in *IEEE Industrial Electronics Magazine*, vol. 8, no. 4, pp. 18-31, Dec. 2014.

[16] H. Tian, X. Wen and Y. W. Li, "A harmonic compensation approach for interlinking voltage source converters in hybrid AC-DC microgrids with low switching frequency," in *CSEE Journal of Power and Energy Systems*, vol. 4, no. 1, pp. 39-48, Mar. 2018.

[17] Ciobotaru, M., Teodorescu, R., Blaabjerg, F.: 'A new single-phase PLL structure based on second order generalised integrator'. Power Electronics Specialists Conf., pp. 1–6, 2006.

[18] S. Taghizadeh, M. J. Hossain and J. Lu, "Enhanced orthogonal signal generator for a single-phase grid-connected converter," in *IET Power Electronics*, vol. 11, no. 15, pp. 2563-2572, Dec. 2018.

[19] W. Feng, K. Sun, Y. Guan, J. M. Guerrero and X. Xiao, "Active Power Quality Improvement Strategy for Grid-Connected Microgrid Based on Hierarchical Control," in *IEEE Transactions on Smart Grid*, vol. 9, no. 4, pp. 3486-3495, Jul. 2018.

[20] S. N. Fallah, M. Ganjkhani, S. Shamshirband, K. W. Chau, "Computational Intelligence on Short-Term Load Forecasting: A Methodological Overview," in *Energies*, vol. 12, no. 3, pp. 393-413, 2019.

[21] M. A. Hammad, B. Jereb, B. Rosi, D. Dragan, "Methods and Models for Electric Load Forecasting: A Comprehensive Review," in *Logistics & Sustainable Transport*, vol. 11, no. 1, pp. 51-76, Feb. 2020.

[22] G. Pandove and M. Singh, "Robust Repetitive Control Design for a Three-Phase Four Wire Shunt Active Power Filter," in *IEEE Transactions on Industrial Informatics*, vol. 15, no. 5, pp. 2810-2818, May 2019.

[23] N. D. Tuyen and G. Fujita, "PV-Active Power Filter Combination Supplies Power to Nonlinear Load and Compensates Utility Current," in *IEEE Power and Energy Technology Systems Journal*, vol. 2, no. 1, pp. 32-42, Mar. 2015.

[24] H. R. Baghaee, M. Mirsalim, G. B. Gharehpetian and H. A. Talebi, "A Decentralised Power Management and Sliding Mode Control Strategy for Hybrid AC/DC Microgrids including Renewable Energy Resources," in *IEEE Transactions on Industrial Informatics*, 2017.

[25] H. R. Baghaee, M. Mirsalim, G. B. Gharehpetian and H. A. Talebi, "Unbalanced harmonic power sharing and voltage compensation of microgrids using radial basis function neural network-based harmonic power-flow calculations for distributed and decentralised control structures," in *IET Generation, Transmission & Distribution*, vol. 12, no. 7, pp. 1518-1530, Apr. 2018.

[26] H. R. Baghaee, M. Mirsalim, G. B. Gharehpetan and H. A. Talebi, "Nonlinear Load Sharing and Voltage Compensation of Microgrids Based on Harmonic Power-Flow Calculations Using Radial Basis Function Neural Networks," in *IEEE Systems Journal*, vol. 12, no. 3, pp. 2749-2759, Sep. 2018.

[27] H. R. Baghaee, M. Mirsalim, G. B. Gharehpetian and H. A. Talebi, "Decentralized Sliding Mode Control of WG/PV/FC Microgrids Under Unbalanced and Nonlinear Load Conditions for On- and Off-Grid Modes," in IEEE Systems Journal, vol. 12, no. 4, pp. 3108-3119, Dec. 2018.

[28] L. B. Garcia Campanhol, S. A. Oliveira da Silva and A. Goedtel, "Application of shunt active power filter for harmonic reduction and reactive power compensation in three-phase four-wire systems," in *IET Power Electronics*, vol. 7, no. 11, pp. 2825-2836, Nov. 2014.

[29] Z. Lin, X. Ruan, L. Jia, W. Zhao, H. Liu and P. Rao, "Optimized Design of the Neutral Inductor and Filter Inductors in Three-Phase Four-Wire Inverter With Split DC-Link Capacitors," in *IEEE Transactions on Power Electronics*, vol. 34, no. 1, pp. 247-262, Jan. 2019.

[30] Y. Zhang, J. Jiao and D. Xu, "Direct Power Control of Doubly Fed Induction Generator Using Extended Power Theory Under Unbalanced Network," in *IEEE Transactions on Power Electronics*, vol. 34, no. 12, pp. 12024-12037, Dec. 2019.

[31] A. Bertani, C. Bossi, F. Fornari, S. Massucco, S. Spelta and F. Tivegna, "A microturbine generation system for grid connected and islanding operation," *IEEE PES Power Systems Conference and Exposition*, vol.1, New York, NY, pp. 360-365, 2004.

[32] Seyedfoad Taghizadeh, M.J. Hossain, Junwei Lu, Wayne Water, "A unified multi-functional on-board EV charger for power-quality control in household networks," *Applied Energy*, vol. 215, pp. 186-201, 2018.

[33] M. S. Rahman, M. J. Hossain, J. Lu and H. R. Pota, "A Need-Based Distributed Coordination Strategy for EV Storages in a Commercial Hybrid AC/DC Microgrid With an Improved Interlinking Converter Control Topology," in *IEEE Transactions on Energy Conversion*, vol. 33, no. 3, pp. 1372-1383, Sep. 2018.